*Terra Nova*

WILEY

Terra Nova

RESEARCH ARTICLE OPEN ACCESS

# Orogenward Migration of the Flexural Forebulge: A Response to Increased (Sub)surface Loading in the Orogenic Core?

Lucas H. J. Eskens | Giridas Maiti | Nevena Andrić-Tomašević

Karlsruhe Institute of Technology, Institute of Applied Geosciences, Karlsruhe, Germany

**Correspondence:** Lucas H. J. Eskens (lucas.eskens@kit.edu; lucas.eskens@witteveenbos.com)

**Received:** 23 October 2024 | **Revised:** 13 July 2025 | **Accepted:** 17 July 2025

**Funding:** This work was supported by Deutsche Forschungsgemeinschaft, TO 1364/1-1.

## ABSTRACT

The flexural profile of a foreland basin is controlled by lower plate strength and the magnitude of (sub)surface loads. Assuming that lower plate strength remains largely constant during flexure, changes in the flexural profile hint at reorganisations of (sub) surface loading. During the early Miocene, the forebulge in the Eastern Northern Alpine Foreland Basin migrated 80 km towards the orogenic front. This change in basin architecture occurred concurrently with intensified folding in the Tauern Window whilst the Eastern Alpine orogenic front ceased to propagate cratonward. Here, we construct 2D flexural models to test whether the resultant focusing of topographic loading into the hinterland, exerted by Tauern Window exhumation, forced orogenward migration of the forebulge. However, our results suggest that solely the focusing of the topographic load cannot explain the observed orogenward propagation of the forebulge. Likely, this requires a contribution of visco-elastic relaxation, supported by changes in subsurface loads during the necking of the European slab.

## 1 | Introduction

Pro-foreland basins, from hereon foreland basins, form adjacent to growing mountain ranges due to the flexural bending of the continental foreland plate (Beaumont 1981; DeCelles and Giles 1996; Roure 2008). The foreland basin system consists of four discrete depozones: the wedge-top, foredeep, forebulge and back-bulge (Figure 1, DeCelles and Giles 1996). Most syn-orogenic deposits are preserved in the foredeep (DeCelles and Giles 1996; DeCelles 2012). The forebulge is a flexural upwarp that marks the cratonward limit of the foredeep (Figure 1, DeCelles 2012). The magnitude of the slab, thrust, and sedimentary loads (Beaumont 1981; Flemings and Jordan 1989; DeCelles and Giles 1996; Sinclair 1997; Fosdick et al. 2014), as well as the mechanical properties of the flexed lower plate (Waschbusch and Royden 1992; Royden 1993) dictate the flexural profile of a foreland basin and, thereby, the position of the forebulge.

The forebulge migrates cratonward as the mountain range encroaches the lower continental plate (Figure 1, Chang et al. 2012; DeCelles 2012; Sabbatino et al. 2021), either continuously or episodically (Waschbusch and Royden 1992; Filer 2003). This migration generates a diachronous unconformity tracing its spatiotemporal location (Crampton and Allen 1995). Apart from cratonward migration, orogenward migration of the forebulge (i.e., the forebulge migrating towards the orogenic front concurrent with basin deepening- and narrowing) has been recognised in various foreland basins (Northern Alpine, Colville, and Appalachian foreland basins, Coakley and Watts 1991; Ver Straeten and Brett 2000; Kuhlemann and Kempf 2002). In essence, this represents a narrowing and enhancement of the amplitude of the flexural response to changes in loading or rigidity of the lower plate. Orogenward migration of the forebulge has been attributed to (1) visco-elastic relaxation of the lower plate (Quinlan and

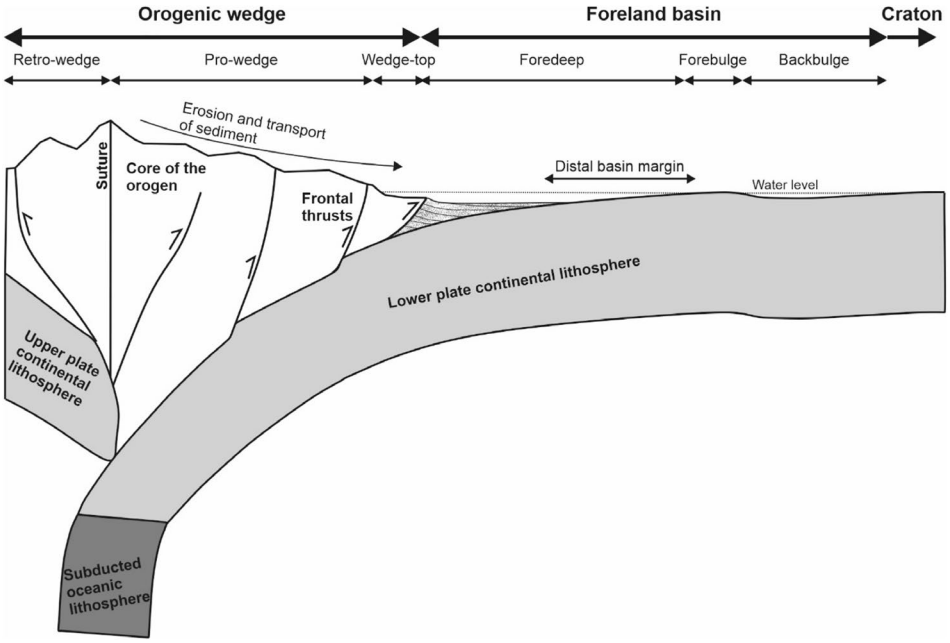


**FIGURE 1** | Schematic representation of the general architecture of a foreland basin and orogenic wedge. The different geological elements are not to scale. The retro-wedge side of the system is only partly drawn. Modified after (Naylor and Sinclair 2008).

Beaumont 1984; Zweigel et al. 1998), (2) onset of in-sequence frontal thrusting after a period of tectonic quiescence (Quinlan and Beaumont 1984; Flemings and Jordan 1990), (3) thickening of the mountain range concurrent with slow in-sequence thrusting (Sinclair et al. 1991; Naylor and Sinclair 2008) or (4) redistribution of subcrustal loading (Garcia-Castellanos et al. 2002).

The Northern Alpine Foreland Basin (NAFB, Figure 2a) developed north of the Alps during the convergence between the European and Adriatic plates (Lemcke 1988; Schmid et al. 1996). During the Aquitanian–Burdigalian transition (~21–20 Ma), the Eastern NAFB narrowed by 80 km whilst the proximal foredeep continued to subside (east of Munich, Figure 2c). This has been interpreted as orogenward migration of the forebulge (Figure 2c, Lemcke 1988; Zweigel et al. 1998; Kuhlemann and Kempf 2002; Eskens et al. 2024), causing the development of the angular Base Hall unconformity (BHU, Zweigel et al. 1998). In the deeper Austrian NAFB, this unconformity was interpreted to have formed due to non-deposition (Hülscher et al. 2019).

Previous authors attributed the narrowing of the Eastern NAFB to the visco-elastic relaxation of the European plate (Zweigel et al. 1998; Hülscher et al. 2019). However, as it may take 10s of millions of years for visco-elastic relaxation to be expressed on a crustal scale (up to 27.5 Myr, Beaumont 1981; Coakley and Watts 1991; Thatcher and Pollitz 2008; Burov 2011), its effect on basin architecture remains debated. Lastly, the switch from in-sequence to break-back thrusting (Covault et al. 2009; Hinsch 2013; Ortner et al. 2015) rules out the other two previously introduced mechanisms for driving the orogenward forebulge migration (Quinlan and Beaumont 1984; Flemings and Jordan 1990; Sinclair et al. 1991; Naylor and Sinclair 2008). Therefore, alternative explanation(s) need to be explored.

The intensification of folding and antiformal doming in the Eastern Alpine core (i.e., Tauern Window, Figure 2b, Rosenberg and Berger 2009; Scharf et al. 2013; Favaro et al. 2015; Rosenberg et al. 2018; Hülscher et al. 2021; Verwater et al. 2021) occurred concurrently with orogenward forebulge migration. The former likely led to a narrowing of the topographic load in the core of the stationary Eastern Alps. We hypothesise that this spatial redistribution of the topographic load, analogously to increasing the torque applied to an elastic beam, led to greater downward flexure of the foreland plate. As a result, the forebulge migrated orogenward. To test the validity of this hypothesis, we constrain changes in the architecture of the Eastern NAFB using reflection seismic data (Figure 2). Subsequently, we construct 2D flexural models to quantitatively investigate the effect of narrowing of the topographic load in the core of a stationary orogen on the position of the forebulge.

## 2 | Geological Background

As our focus is Aquitanian-Burdigalian transition, we do not give an in-depth description of the entire evolution of the Alps-NAFB system. For a complete synopsis, the reader is referred to other contributions (Lemcke 1988; Schmid et al. 1996; Kuhlemann and Kempf 2002; Handy et al. 2010; Ortner et al. 2023; Eskens et al. 2024).

### 2.1 | The Alpine Orogenic Wedge

The Alps are a stack of Adria- and Europe-derived nappes that document the closure of the Alpine Tethys (Penninic and Valais domains, e.g., Trümpy 1960; Schmid et al. 1996; Handy et al. 2010). From the late Eocene to the early Miocene, the Alps overthrusted and incorporated the European continental margin (Helvetic domain) and the Subalpine Molasse (Pfiffner 1986;

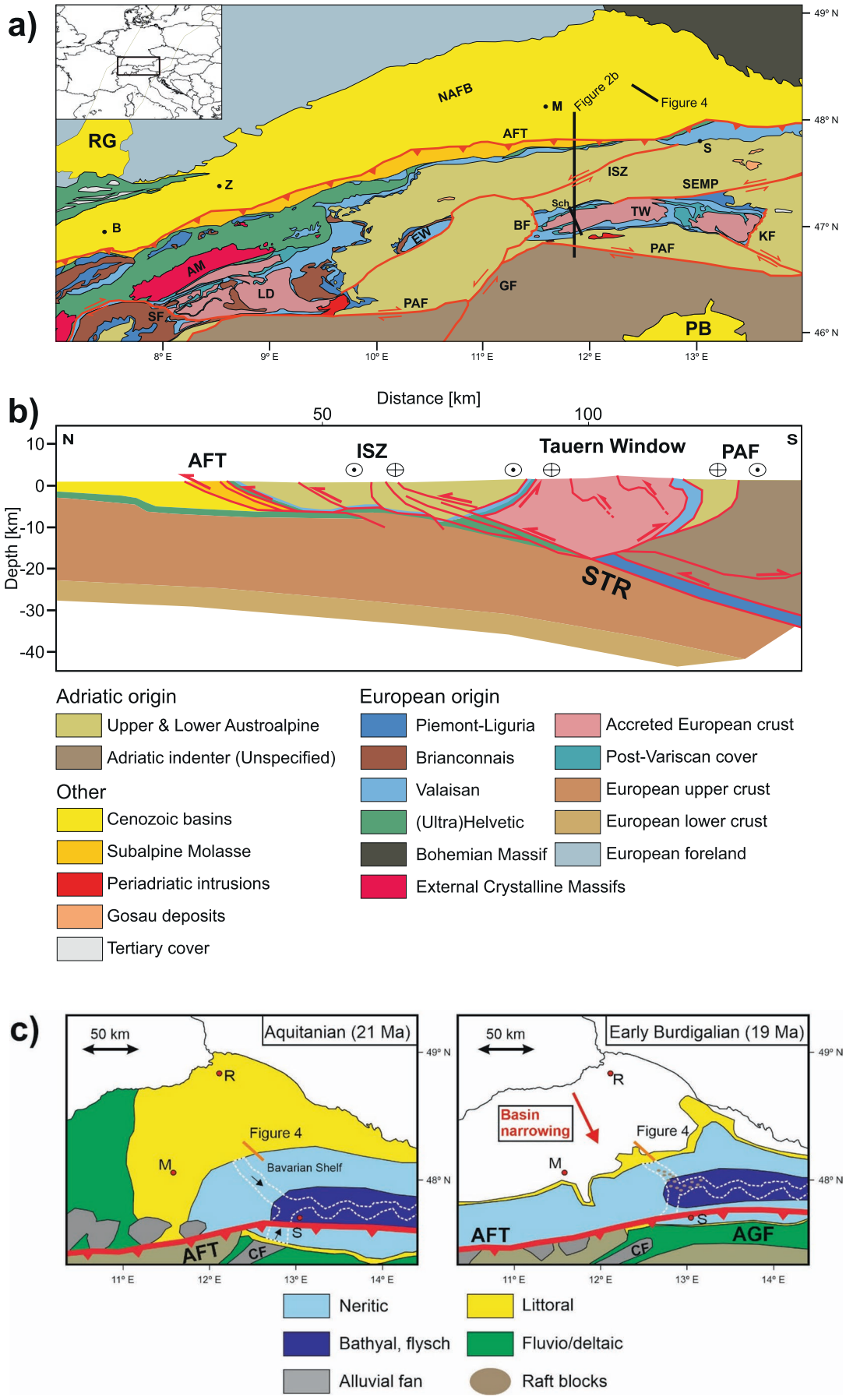


**FIGURE 2** | Legend on next page.

**FIGURE 2** | (a) Present-day geological map of the Northern Alpine Foreland Basin (NAFB) and Eastern and Central Alps. B = Bern, M = Munich, S = Salzburg, Z = Zürich, AFT = Alpine Frontal Thrust, AM = Aar Massif, BF = Brenner Fault, EW = Engadine Window, GF = Giudicaria Fault, ISZ = Inntal Shear Zone, KF = Katschberg Fault, LP = Lepontine Dome, NAFB = Northern Alpine Foreland Basin, PB = Po Basin, PAF = Periadriatic Fault, RG = Rhine Graben, SEMP = Salzach-Ennstal-Mariazell-Puchberg Fault, SF = Simplon Fault, STR = Sub-Tauern Ramp, TW = Tauern Window (b) North–south cross section through the proximal Eastern NAFB and Eastern Alps north of the PAF. Modified from Figure 8 from (Ortner et al. 2006). The internal structure of the Tauern Window is based on cross Section 3 from (Schmid et al. 2013), their Figure 3b. Sch = location of cross Section 3 from Schmid et al. (2013). (c) Paleogeographic reconstructions of the Aquitanian and early Burdigalian NAFB. White dashed lines delineate the meandering Puchkirchen channel belt in the Austrian NAFB, with the black arrows indicating the flow direction. Modified from (Eskens et al. 2024). AGF = Augenstein Formation, CF = Chiemgau Fann. [Colour figure can be viewed at wileyonlinelibrary.com]

Hinsch 2013; Ortner et al. 2023). The early Miocene switch from in-sequence to break-back thrusting in the Eastern Alps (Hinsch 2013; Ortner et al. 2015) evidences the cessation of cratonward propagation. Coevally, the intensification of folding in the Tauern Window (attributed to Adriatic indentation and leading to enhanced exhumation, Fügenschuh et al. 1997; Frisch et al. 2001; Hülscher et al. 2021; Verwater et al. 2021) likely resulted in the narrowing of the topographic load in the Eastern Alpine core. Alternatively, and not mutually exclusive, early Miocene European slab breakoff (Schmid et al. 2004a) was suggested to have enhanced the exhumation of the Tauern Window (Handy et al. 2015). Additionally, some compressional strain was accommodated through eastward tectonic extrusion (Ratschbacher, Frisch, et al. 1991; Ratschbacher, Merle, et al. 1991; Rosenberg et al. 2018).

### 2.2 | The Northern Alpine Foreland Basin

During the Aquitanian, sediments derived from the Western NAFB (west of Munich, Figure 2c) were transported eastward across the Bavarian Shelf (Figure 2c, Jin et al. 1995; Zweigel et al. 1998) into the deep marine Puchkirchen channel belt in the Eastern NAFB (east of Munich, Figure 2c, Wagner 1998; De Ruig and Hubbard 2006; Masalimova et al. 2015). Additionally, sediments derived from the Central Alps were transported to the Eastern NAFB through the Paleo Inn Valley to the Chiemgau Fan (Figure 2c, Frisch et al. 2001; De Ruig and Hubbard 2006; Kuhlemann et al. 2006).

During the Aquitanian-Burdigalian transition (ca. 21–20 Ma), uplift of the distal margin and development of the BHU record 80 km of narrowing of the Eastern NAFB (Figure 2c, Lemcke 1988; Zweigel et al. 1998; Kuhlemann and Kempf 2002). Coevally, the proximal foredeep continued to subside (Zweigel et al. 1998; Genser et al. 2007), and up to 500 m wide raft blocks (sourced from the Bavarian Shelf, Grunert et al. 2013; Hülscher et al. 2019; Borzi et al. 2022) were deposited in the sediment-starved Puchkirchen channel belt just above the BHU (Figure 2c, Hubbard et al. 2009; Hülscher et al. 2019). However, by the middle Burdigalian, deposition again reached as far north as the present-day location of the forebulge (Andeweg and Cloetingh 1998; Kuhlemann and Kempf 2002). Post-Early Miocene uplift of the Eastern NAFB (Gusterhuber et al. 2012) coeval with the continued subsidence of the Western NAFB (Ortner et al. 2015, 2023) led to a reversal from eastward to westward drainage (Kuhlemann and Kempf 2002; Garefalakis and Schlunegger 2019).

## 3 | Data and Methods

### 3.1 | Seismic Data

The seismic data presented in this study is a 2D PreSTM (prestack time migrated) line east of Munich (Figure 2a,c) extracted from seismic data volume B presented in Eskens et al. (2024). The structural smoothing seismic attribute was applied to improve the signal-to-noise ratio. Subsequently, a time-to-depth conversion was made (See Appendix A.1 for details) to obtain real instead of apparent geometries. On the depth-converted seismic data, six reflectors were picked, which are from top to bottom: the top Hall Fm., the BHU (Zweigel et al. 1998; De Ruig and Hubbard 2006; Hülscher et al. 2019), the top Chattian Sands, the top Mesozoic, the top Turonian, and the base Mesozoic (Figure 3). Well data constrain the upper five horizons, while the base Mesozoic is interpreted based on a downward change in seismic facies corresponding with a high positive amplitude reflector (Figure 3).

### 3.2 | Flexural Modelling

The foreland plate is generally treated as a linear elastic solid in flexural modelling on short timescales (< 20–30 Myr; Sinclair et al. 1991). For a static load on a linear elastic plate, the geometry of deflection remains unchanged through time. In contrast, on a viscoelastic plate, the geometry of deflection narrows and deepens with time (Quinlan and Beaumont 1984). Previous studies have applied both types of plate rheology to flexural modelling of foreland basins (Quinlan and Beaumont 1984; Sinclair et al. 1991; Naylor and Sinclair 2008). In this work, we consider a linear elastic plate rheology as we focus on short timescales during which basin architecture changes occur (2 Myrs, Figure 1c).

To evaluate how narrowing of the topographic load within the orogenic core of a stationary orogen influences foreland basin architecture, we apply the semi-numerical solution of Wangen (2010). This allows us to simulate the deflection of elastic foreland plate subjected to a distributed mountain load (Wangen 2010; Allen and Allen 2013, see Appendix A.2). Here, the mountain load is turned into a series of crustal columns of different heights located at discrete intervals (Appendix A.2 and Figure A1). We only increase the topographic load in the core of the orogen (Figure 1) while keeping the orogenic front stationary. We first model the flexural profile of the NAFB with an initial mountain range topography of 500 m (model M500) to represent the Aquitanian "hilly" Eastern Alpine paleotopography (i.e.,

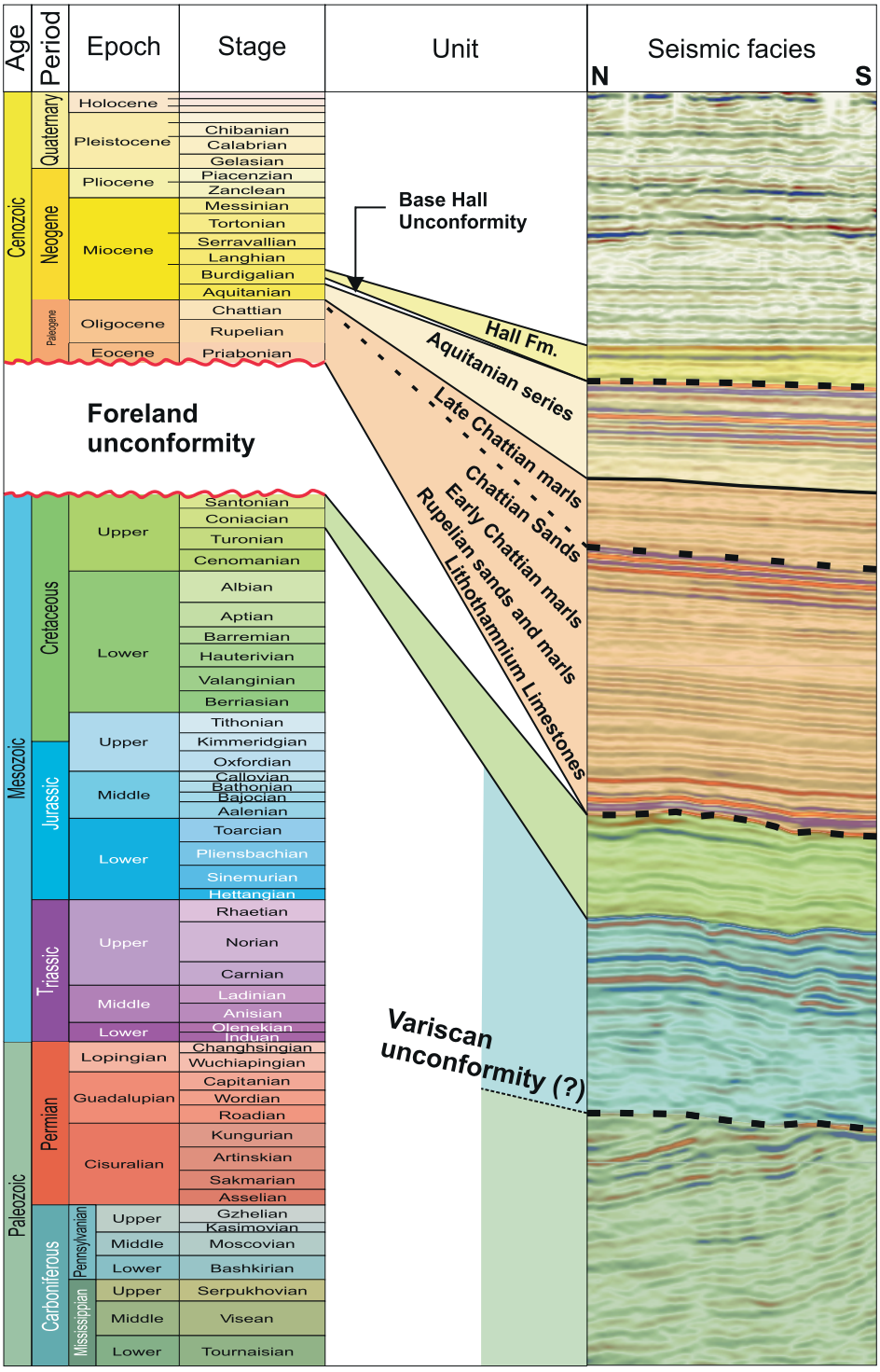


**FIGURE 3** | Seismic-stratigraphic chart of the interpreted data. Ages of the pre-Turonian Mesozoic and Palaeozoic stratigraphy are not constrained. Ages and units overlying the foreland unconformity are as defined by previous studies in the same study area (Jin et al. 1995; Zweigel et al. 1998). [Colour figure can be viewed at wileyonlinelibrary.com]

before basin narrowing, Frisch et al. 1998). In the second stage, we increase the topographic height to 1500 m (model M1500), representing the paleoaltitude in the Eastern Alps at the start of the Burdigalian (estimated to have been 900 to 1800 m, Jiménez-Moreno et al. 2008). Finally, we increase the topographic height to 3000 m (model M3000), which is the suggested Burdigalian peak elevation following the intensified folding of the Tauern Window (Kuhlemann 2007). Assuming the European foreland plate behaves as a linear elastic, Andeweg and Cloetingh (1998) conducted detailed parametric studies to obtain best-fits flexural parameters, which we have used to model the change in flexural deflections of the NAFB. The best-fit flexural rigidity ($D$) value of the European plate lies between $1\times10^{23}$ to $2\times10^{23}$ Nm (Gutscher 1995; Andeweg and Cloetingh 1998). The flexural rigidity $D$ depends on the elastic thickness ($h$), Young's modulus ($E$), and Poisson's ratio ($\nu$) of the elastic plate (Appendix A.2).

**TABLE 1** | List of flexural simulations and respective parameters.

| Model name | Orogenic core topography [m] | Occurrence of visco-elastic relaxation [yes/no] | Lower plate flexural rigidity [Nm] | Mantle density [kg m$^{-3}$] | Crustal density [kg m$^{-3}$] |
|---|---|---|---|---|---|
| M500 | 500 | No | $2\times10^{23}$ | 3300 | 2750 |
| M1500 | 1500 | No | $2\times10^{23}$ | 3300 | 2750 |
| M3000 | 3000 | No | $2\times10^{23}$ | 3300 | 2750 |
| M3000-R | 3000 | Yes | $1\times10^{23}$ | 3300 | 2750 |

Taking the standard values of $E=70$ GPa and $\nu=0.25$ (Cardozo and Jordan 2001) for a continental plate, this translates to elastic thickness of the European plate between 26 to 31 km. In all flexural models (M500, M1500 and M3000; Table 1), we use a flexural rigidity ($D$) of $2\times10^{23}$ Nm. However, to assess the first-order effects of viscoelastic relaxation on flexural response, we reduced the rigidity ($D$) to $1\times10^{23}$ Nm in the final model (M3000-R), after 3000 m of topography developed in the orogenic core. Although the model is purely elastic, we approximate viscoelastic relaxation by lowering the flexural rigidity. This simplification is due to uncertainties in both the extent of rigidity reduction and relaxation timescales. Nonetheless, the reduced $D$ value remains within the estimated range of flexural rigidity for the European foreland plate (Andeweg and Cloetingh 1998), and it captures the first-order influence of viscoelastic behaviour. Additionally, we use standard values for the densities of the mantle (3300 kg m$^{-3}$) and crust (2750 kg m$^{-3}$) (Gutscher 1995; Andeweg and Cloetingh 1998; Maiti et al. 2024).

## 4 | Results

### 4.1 | Seismic Interpretations

This contribution focuses on the changes in basin architecture in the Eastern NAFB during the early Miocene Aquitanian to Burdigalian transition (ca. 21-20 Ma). For pre-Aquitanian stratigraphy, the reader is referred to Eskens et al. (2024).

The Aquitanian seismic-stratigraphy consists of high-amplitude parallel reflectors with good lateral continuity (Figure 4a). In the SE of the seismic line, Aquitanian reflectors terminate against the BHU (Figure 4b). We interpret this to present an erosional truncation resulting from incision. Overlying early Burdigalian seismic-stratigraphy is characterised by laterally continuous medium to low amplitude reflectors (Figure 4a). In the SE of the seismic line, early Burdigalian reflectors onlap towards the NW onto the BHU (Figure 4b). This implies that during the Aquitanian–Burdigalian transition, deposition was initially restricted to the basin axis, reaching progressively further north.

### 4.2 | Flexural Modelling Results

For model M500 (500 m high orogen, Figure 5a), the resulting flexural profile shows a 180 km wide, 1.25 km deep foredeep bounded by an 80 m high forebulge (Figure 5a). Subsequently, the hinterland topography is increased to 1500 m whilst the orogenic front remains stationary (model M1500, Figure 5b). This results in 18 km of orogenward migration of the forebulge accompanied with 115 m of vertical uplift (Figure 5b). Furthermore, the foredeep depth increases by 1.4 km to 2.65 km (Figure 5b). Finally, an increase of hinterland topography to 3000 m results in an additional 10 km of orogenward forebulge migration concurrent with 98 m uplift of its crest (model M3000, Figure 5c). Moreover, the foredeep deepens by 0.85 km to a final depth of 3.5 km (Figure 5c). When visco-elastic relaxation is allowed (model M3000-R), the forebulge migrates 40 km orogenward whilst its crest is uplifted by 110 m (Figure 5c). This suggests visco-elastic relaxation leads to an additional 30 km of orogenward migration of the forebulge compared to the model without relaxation (M3000). Overall, all the models reveal a progressive steepening of the distal basin margin (Figure 1) as the topographic load increases in the orogenic core, whilst the mountain front remains stationary (irrespective of whether visco-elastic relaxation occurs or not, Figure 5). Lastly, the cumulative orogenward forebulge migration reaches up to 68 km (Figure 5).

## 5 | Discussion

Seismic-reflection data north of the Tauern Window revealed early Burdigalian reflectors terminating against the BHU (Figures 2a and 4). This can be interpreted as follows:

1. The incision into Aquitanian distal basin margin sediments, followed by subsequent renewed deposition resulting in onlapping during the early Burdigalian.
2. The incision by- and subsequent filling of a channel (belt) on the distal basin margin.

The first interpretation suggests that Aquitanian sediments were eroded by southward oversteepening of the distal basin margin due to orogenward forebulge migration, in agreement with previous authors (Zweigel et al. 1998; Kuhlemann and Kempf 2002). This is similar to the formation of the NSU in the Austrian Molasse (Masalimova et al. 2015; Hülscher et al. 2019). For the second interpretation, steepening of the distal basin margin due to orogenward forebulge migration may have enabled a high-energy channel (belt) to erode former distal margin deposits. Either way, both interpretations advocate the steepening and remobilisation of sediments on the distal margin. Deposition of this material as raft blocks in the Puchkirchen channel belt just above the BHU (Figure 2c,

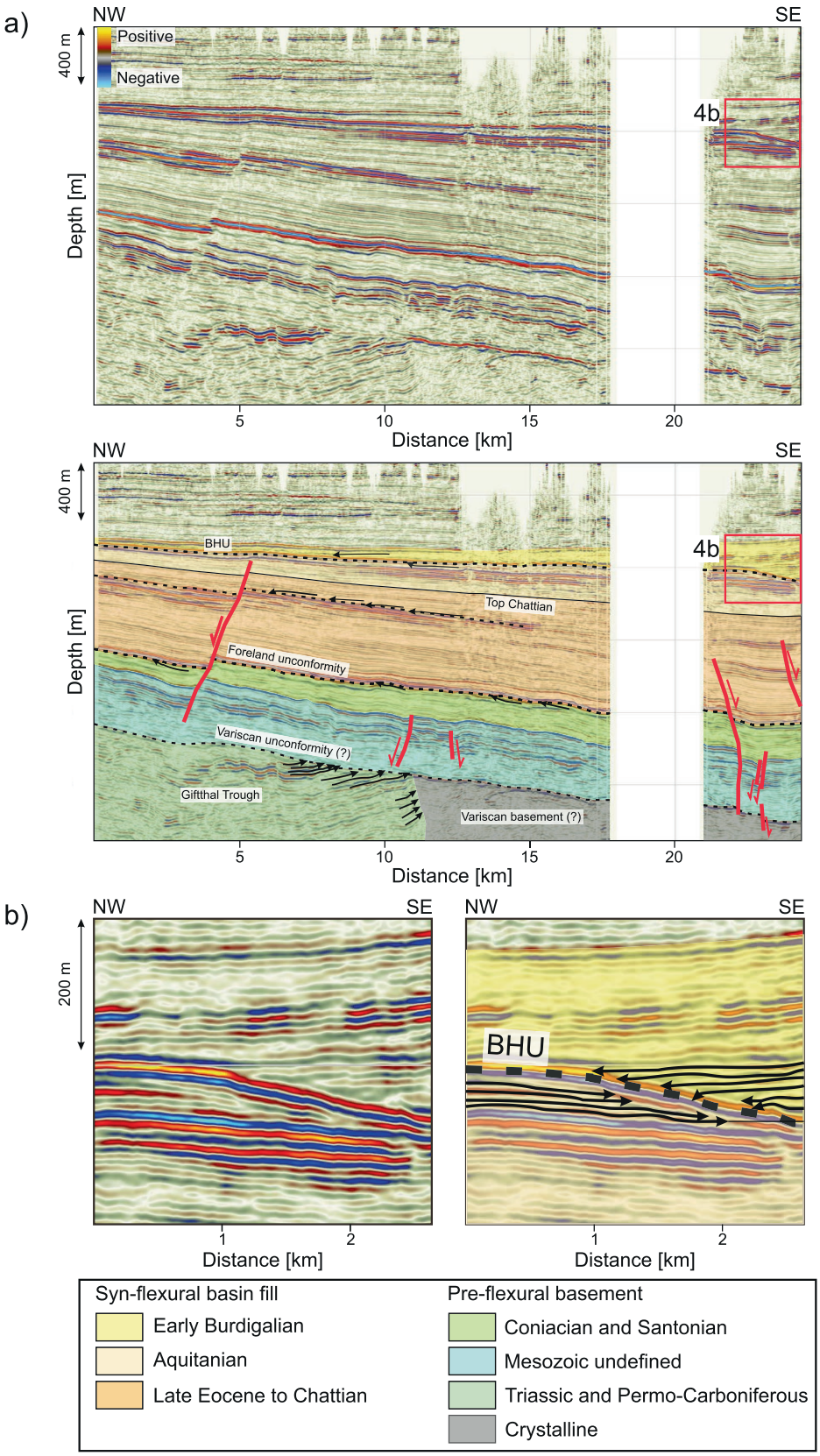


**FIGURE 4** | (a) The upper panel shows an uninterpreted NW-SE seismic line across the Bavarian Shelf, and the lower panel shows an interpreted version of the same seismic line. Red lines indicate normal faults and their respective kinematics, black dashed lines indicate unconformities. (b) Uninterpreted and interpreted part of the NW-SE seismic line. Below BHU, the arrows mark Aquitanian reflector terminations due to incision; above BHU, the black arrows mark subsequent early Burdigalian onlapping. [Colour figure can be viewed at wileyonlinelibrary.com]

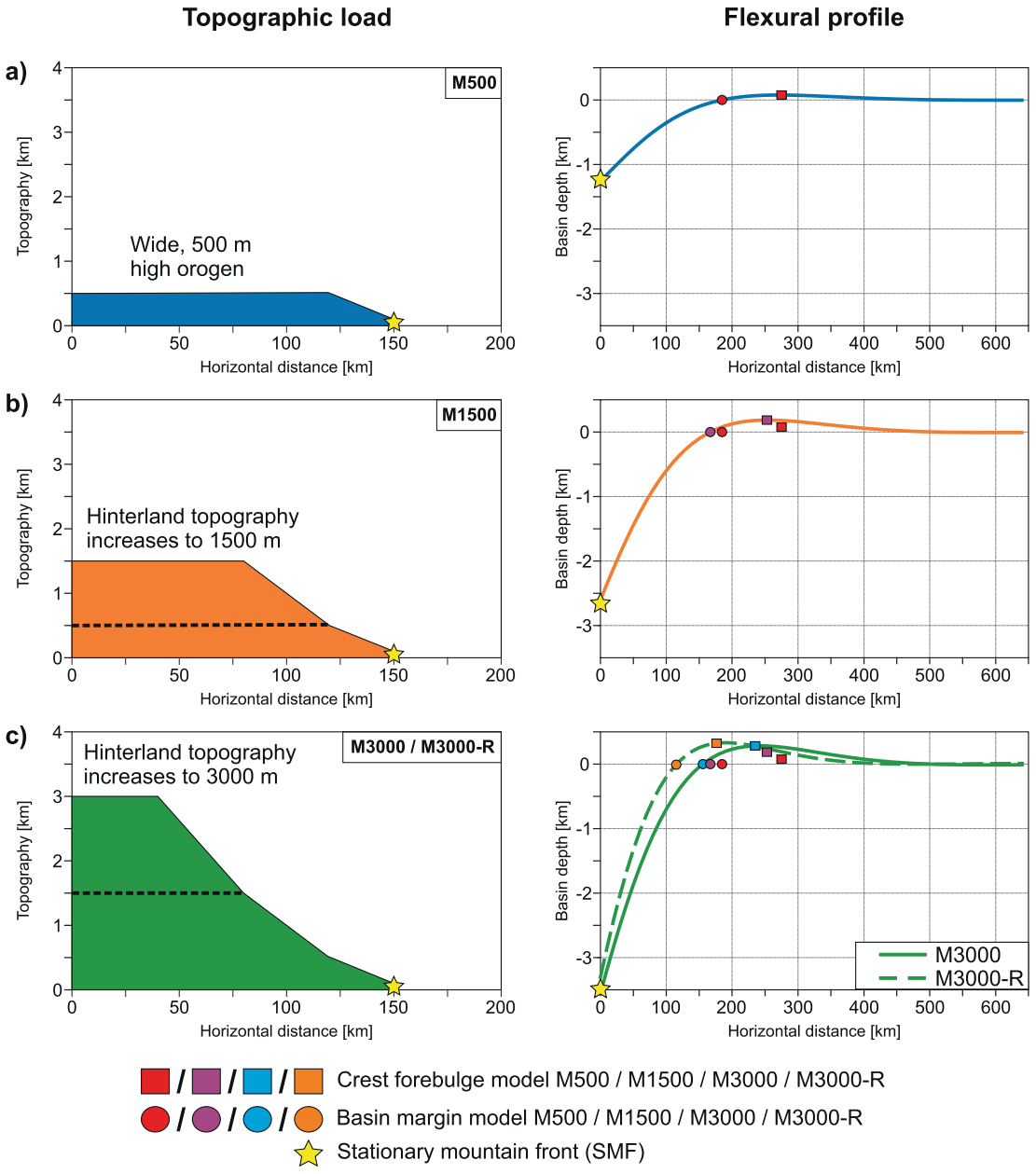


**FIGURE 5** | Three different scenarios of topographic load distribution in the orogen and respective flexural profile of the adjacent foreland for models (a) M500, (b) M1500, (c) M3000 and M3000-R. For the topographic loads, the coloured area above the dashed line represents the added topographic load between the respective steps. [Colour figure can be viewed at wileyonlinelibrary.com]

Hubbard et al. 2009; Borzi et al. 2022) hints at slope collapse rather than gradual erosion.

Our modelling suggests narrowing of the topographic load in the core of a stationary orogen, resembling the early Miocene amplified antiformal doming in the Tauern Window attributed to Adriatic indentation (Frisch et al. 2001; Hülscher et al. 2021; Verwater et al. 2021), leads to orogenward forebulge migration (Figures 5 and 6a). Although the stacking and folding of the Tauern Window had already initiated in the Oligocene (e.g., Schmid et al. 2013 and references therein), subsequent narrowing of the accreted material during the early Miocene enhanced the deflection of the lower plate. Subsequent tectonic exhumation, erosion and eastward lateral escape (Ratschbacher, Frisch, et al. 1991; Kuhlemann and Kempf 2002; Hülscher et al. 2021) would result in unloading and, thereby, northward migration of the forebulge to its present-day location (Andeweg and Cloetingh 1998). However, in models resembling antiformal doming of the Tauern Window, forebulge migration only reached 28 km (model M3000, Figure 5). Incorporating visco-elastic relaxation led to an increase of this migration to 68 km (Model M3000-R, Figures 5 and 6b), broadly comparable to what is observed in the Eastern Molasse (80 km, Figure 2c).

However, a caveat remains: the orogenward forebulge migration is predominantly caused by visco-elastic relaxation (Figure 5c). Notably, visco-elastic relaxation is associated with

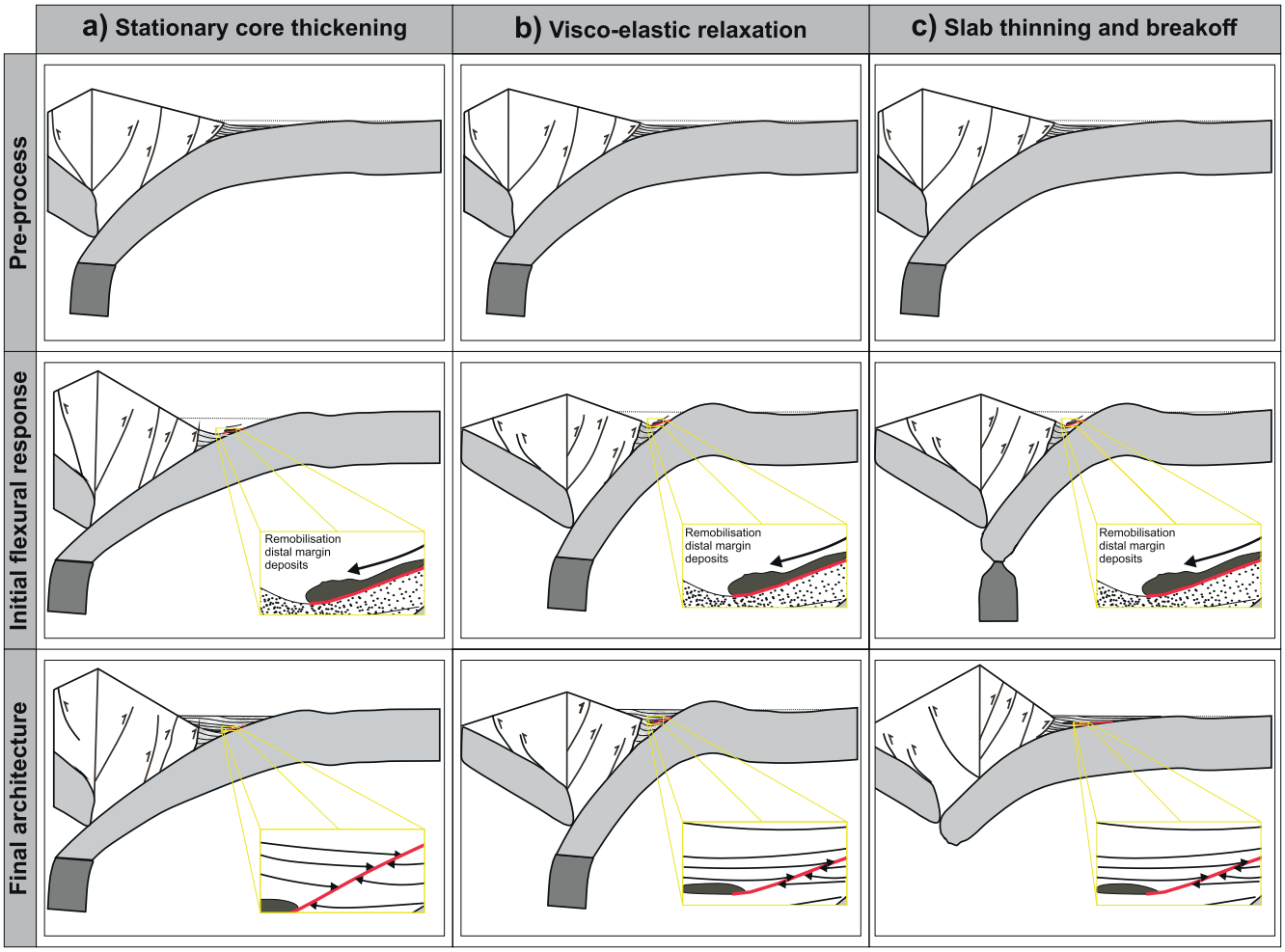


**FIGURE 6** | (a) Schematic representation of the effect of thickening of the core of a stationary orogen on the architecture of a foreland basin. Initially, the extra thrust loading results in a slight uplift of the forebulge and steepening of the distal margin. This causes remobilisation and redeposition of synorogenic distal basin margin sediments downslope in the basin axis. However, the orogenward migration of the forebulge is small. Subsequent deposition will onlap onto the erosional surface generated by the steepening of the distal basin margin. (b) Schematic representation of visco-elastic relaxation on the architecture of a foreland basin. Visco-elastic relaxation results in both uplift and significant orogenward migration of the forebulge, concurrent with subsidence of the mountain range. The former causes steepening of the distal basin margin, resulting in remobilisation of distal sediments and redeposition in the basin axis. However, due to the latter, the diminished topography of the orogenic wedge leads to a decrease in sediment supply. Together, this leads to underfilling of the basin. Sediments deposited following visco-elastic relaxation will onlap onto the erosional surface generated by distal margin steepening. However, following visco-elastic relaxation, the forebulge remains at a stationary position (in the absence of other processes). (c) Schematic representation of the effect of slab necking and breakoff on the architecture of a foreland basin. During slab necking, enhanced loading through increased slab pull causes orogenward migration and uplift of the forebulge. As a result, the distal basin margin oversteepens, and foreland deposits are remobilised and redeposited further downslope in the basin axis. This causes the formation of an unconformity onto which post-breakoff deposits onlap. Furthermore, because of isostatic rebound of the mountain range, sediment supply increases, leading to overfilling of the basin. Unloading of the lower plate through slab breakoff also allows cratonward migration of the forebulge and a decrease of its amplitude following the initial orogenward migration. [Colour figure can be viewed at wileyonlinelibrary.com]

periods of tectonic quiescence (Quinlan and Beaumont 1984; Flemings and Jordan 1990). This does not fit with post-Aquitanian Eastern Alpine break-back thrusting (Covault et al. 2009; Hinsch 2013; Ortner et al. 2015). Moreover, previous studies have found that it may take between 5 to 27.5 Myrs for visco-elastic relaxation to express itself on basin scale (Beaumont 1981; Coakley and Watts 1991; Thatcher and Pollitz, 2008; Burov, 2011). This does not corroborate with the changes in the NAFB architecture only lasting 1–2 Myrs (Figure 2c). Because of these shortcomings, additional processes need to be considered to have played a role in the orogenward forebulge migration.

Numerical modelling has shown that during slab necking (a short phase before breakoff), subsidence of the orogen and foreland drastically increases (Duretz et al. 2012; Eskens 2025; Piccolo et al. 2025). This results from the increase in pull from the slab as its attachment to the lower plate progressively thins, followed by breakoff within 1–2 Myrs (Gerya et al. 2004; Duretz et al. 2012; Schellart 2017; Piccolo et al. 2025). With this process in mind, we suggest that the slab load acting on the European plate increased shortly before early Miocene slab breakoff (Figure 6c, Schmid et al. 2004b; Handy et al. 2015). The breakoff then released the pull force, resulting in unloading and isostatic rebound of the lower plate (e.g., Maiti et al. 2024). This caused

an increase in wavelength and a decrease in amplitude of the flexural profile, allowing the forebulge to migrate north to its present-day location (Figure 6c, Andeweg and Cloetingh 1998). Furthermore, it caused post-early Miocene uplift of the Eastern NAFB (Gusterhuber et al. 2012) while the Western NAFB continued to subside (Ortner et al. 2015, 2023) due to continued European subduction. This suggests that along-strike variations in slab dynamics control foreland flexure, as also demonstrated by recent numerical models of slab tearing in collisional settings (Maiti et al. 2024).

## 6 | Conclusions

Seismic data north of the Tauern Window, integrated with previous observations, indicate erosion (and possibly collapse) of the distal margin of the Eastern NAFB during the Aquitanian-Burdigalian transition. This was likely caused by orogenward forebulge migration. 2D flexural models show that narrowing of the topographic load in the orogenic core alone, mimicking early Miocene intensified folding in the Tauern Window, cannot explain the magnitude of this orogenward forebulge migration. Whilst models including visco-elastic relaxation better match the observed orogenward forebulge migration, the time it takes for this process to express itself in the basin architecture remains debated. Therefore, we propose that the increase in pull from the European slab during necking contributed to the short-lived changes in the architecture of the Eastern NAFB (i.e., orogenward migration of the forebulge). This suggests that subsurface loads play a key role in shaping foreland basin architecture.


### Acknowledgements

This study was supported by the Deutsche Forschungsgemeinschaft (DFG) grant to Nevena Andrić-Tomašević (TO 1364/1-1). We want to thank ONEO GmbH & Co. KG for providing and allowing us to publish the seismic data presented in this study, visualised using the free version of OpendTect 7.0. Figures were prepared using the 2021 version of Coreldraw. The content of this manuscript benefited from discussions with Anne Bernhardt (FU Berlin), Arthur Borzi (FU Berlin), and Mark Handy (FU Berlin). Open Access funding enabled and organized by Projekt DEAL.


### Conflicts of Interest

The authors declare no conflicts of interest.

### Data Availability Statement

The reflection seismic data that support the findings of this study are available from ONEO GmbH. Restrictions apply to the availability of these reflection seismic data, which were used under license for this study. Data are not available from the author(s) and permission/access should be requested of ONEO GmbH. The code for the flexural modeling is available on request.

### References


Allen, P. A., and J. R. Allen. 2013. *Basin Analysis: Principles and Application to Petroleum Play Assessment*. John Wiley & Sons.

Andeweg, B., and S. Cloetingh. 1998. "Flexure and 'Unflexure' of the North Alpine German-Austrian Molasse Basin: Constraints From Forward Tectonic Modelling." *Geological Society, London, Special Publications* 134, no. 1: 403–422.

Beaumont, C. 1981. "Foreland Basins." *Geophysical Journal International* 65, no. 2: 291–329.

Borzi, A., P. McPhee, J. Hülscher, E. LeBreton, M. R. Handy, and A. Bernhard. 2022. "Major Neogene Shift in the Structural and Sedimentary Evolution of the North Alpine Foreland Basin." 6th Annual AlpArray Scientific Meeting, Prague.

Burov, E. B. 2011. "Rheology and strength of the lithosphere." *Marine and petroleum Geology* 28, no. 8: 1402–1443.

Cardozo, N., and T. Jordan. 2001. "Causes of Spatially Variable Tectonic Subsidence in the Miocene Bermejo Foreland Basin, Argentina." *Basin Research* 13, no. 3: 335–357.

Chang, J.-H., H.-S. Yu, H.-H. Hsu, and C.-S. Liu. 2012. "Forebulge Migration in Late Cenozoic Western Taiwan Foreland Basin." *Tectonophysics* 578: 117–125.

Coakley, B. J., and A. B. Watts. 1991. "Tectonic Controls on the Development of Unconformities: The North Slope, Alaska." *Tectonics* 10, no. 1: 101–130.

Covault, J. A., S. M. Hubbard, S. A. Graham, R. Hinsch, and H.-G. Linzer. 2009. "Turbidite-Reservoir Architecture in Complex Foredeep-Margin and Wedge-Top Depocenters, Tertiary Molasse Foreland Basin System, Austria." *Marine and Petroleum Geology* 26, no. 3: 379–396.

Crampton, S., and P. Allen. 1995. "Recognition of Forebulge Unconformities Associated With Early Stage Foreland Basin Development: Example From the North Alpine Foreland Basin." *AAPG Bulletin* 79, no. 10: 1495–1514.

De Ruig, M. J., and S. M. Hubbard. 2006. "Seismic Facies and Reservoir Characteristics of a Deep-Marine Channel Belt in the Molasse Foreland Basin, Puchkirchen Formation, Austria." *AAPG Bulletin* 90, no. 5: 735–752.

DeCelles, P. G. 2012. *Foreland Basin Systems Revisited: Variations in Response to Tectonic Settings*, 405–426. Tectonics of sedimentary basins.

DeCelles, P. G., and K. A. Giles. 1996. "Foreland Basin Systems." *Basin Research* 8, no. 2: 105–123.

Duretz, T., S. Schmalholz, and T. Gerya. 2012. "Dynamics of Slab Detachment." *Geochemistry, Geophysics, Geosystems* 13, no. 3: 2011GC004024.

Eskens, L. H. 2025. "On the Mechanisms Controlling Along-Strike Variations in Pro-Foreland Basin Development: A Case Study of the Alps-Molasse Basin System." Kalrsruhe Institute for Technology, KITOpen.

Eskens, L. H., N. Andrić-Tomašević, P. M. Süss, M. Müller, R. Herrmann, and T. A. Ehlers. 2024. "Lithospheric-and Crustal-Scale Controls on Variations in Foreland Basin Development in the Northern Alpine Foreland Basin." *Tectonophysics* 878: 230283.

Favaro, S., R. Schuster, M. R. Handy, A. Scharf, and G. Pestal. 2015. "Transition From Orogen-Perpendicular to Orogen-Parallel Exhumation and Cooling During Crustal Indentation—Key Constraints From 147Sm/144Nd and 87Rb/87Sr Geochronology (Tauern Window, Alps)." *Tectonophysics* 665: 1–16.

Filer, J. K. 2003. "Stratigraphic Evidence for a Late Devonian Possible Back-Bulge Basin in the Appalachian Basin, United States." *Basin Research* 15, no. 3: 417–429.

Flemings, P. B., and T. E. Jordan. 1989. "A Synthetic Stratigraphic Model of Foreland Basin Development." *Journal of Geophysical Research: Solid Earth* 94, no. B4: 3851–3866.

Flemings, P. B., and T. E. Jordan. 1990. "Stratigraphic Modeling of Foreland Basins: Interpreting Thrust Deformation and Lithosphere Rheology." *Geology* 18, no. 5: 430–434.

Fosdick, J. C., S. A. Graham, and G. E. Hilley. 2014. "Influence of Attenuated Lithosphere and Sediment Loading on Flexure of the Deep-Water Magallanes Retroarc Foreland Basin, Southern Andes." *Tectonics* 33, no. 12: 2505–2525.

Frisch, W., J. Kuhlemann, I. Dunkl, and A. Brügel. 1998. "Palinspastic Reconstruction and Topographic Evolution of the Eastern Alps During Late Tertiary Tectonic Extrusion." *Tectonophysics* 297, no. 1–4: 1–15.

Frisch, W., J. Kuhlemann, I. Dunkl, and B. Székely. 2001. "The Dachstein Paleosurface and the Augenstein Formation in the Northern Calcareous Alps—A Mosaic Stone in the Geomorphological Evolution of the Eastern Alps." *International Journal of Earth Sciences* 90: 500–518.

Fügenschuh, B., D. Seward, and N. Mancktelow. 1997. "Exhumation in a Convergent Orogen: The Western Tauern Window." *Terra Nova* 9, no. 5–6: 213–217.

Garcia-Castellanos, D., M. Fernandez, and M. Torné. 2002. "Modeling the Evolution of the Guadalquivir Foreland Basin (Southern Spain)." *Tectonics* 21, no. 3: 9-1–9-17.

Garefalakis, P., and F. Schlunegger. 2019. "Tectonic Processes, Variations in Sediment Flux, and Eustatic Sea Level Recorded by the 20 Myr Old Burdigalian Transgression in the Swiss Molasse Basin." *Solid Earth* 10, no. 6: 2045–2072.

Genser, J., S. A. Cloetingh, and F. Neubauer. 2007. "Late Orogenic Rebound and Oblique Alpine Convergence: New Constraints From Subsidence Analysis of the Austrian Molasse Basin." *Global and Planetary Change* 58, no. 1–4: 214–223.

Gerya, T. V., D. A. Yuen, and W. V. Maresch. 2004. "Thermomechanical Modelling of Slab Detachment." *Earth and Planetary Science Letters* 226, no. 1–2: 101–116.

Grunert, P., R. Hinsch, R. F. Sachsenhofer, et al. 2013. "Early Burdigalian Infill of the Puchkirchen Trough (North Alpine Foreland Basin, Central Paratethys): Facies Development and Sequence Stratigraphy." *Marine and Petroleum Geology* 39, no. 1: 164–186.

Gusterhuber, J., I. Dunkl, R. Hinsch, H.-G. Linzer, and R. Sachsenhofer. 2012. "Neogene Uplift and Erosion in the Alpine Foreland Basin (Upper Austria and Salzburg)." *Geologica Carpathica* 63, no. 4: 295–305.

Gutscher, M.-A. 1995. "Crustal Structure and Dynamics in the Rhine Graben and the Alpine Foreland." *Geophysical Journal International* 122, no. 2: 617–636.

Handy, M. R., S. M. Schmid, R. Bousquet, E. Kissling, and D. Bernoulli. 2010. "Reconciling Plate-Tectonic Reconstructions of Alpine Tethys With the Geological–Geophysical Record of Spreading and Subduction in the Alps." *Earth-Science Reviews* 102, no. 3–4: 121–158.

Handy, M. R., K. Ustaszewski, and E. Kissling. 2015. "Reconstructing the Alps–Carpathians–Dinarides as a Key to Understanding Switches in Subduction Polarity, Slab Gaps and Surface Motion." *International Journal of Earth Sciences* 104, no. 1: 1–26.

Hinsch, R. 2013. "Laterally Varying Structure and Kinematics of the Molasse Fold and Thrust Belt of the Central Eastern Alps: Implications for Exploration." *AAPG Bulletin* 97, no. 10: 1805–1831.

Hubbard, S. M., M. J. de Ruig, and S. A. Graham. 2009. "Confined Channel-Levee Complex Development in an Elongate Depo-Center: Deep-Water Tertiary Strata of the Austrian Molasse Basin." *Marine and Petroleum Geology* 26, no. 1: 85–112.

Hülscher, J., G. Fischer, P. Grunert, G. Auer, and A. Bernhardt. 2019. "Selective Recording of Tectonic Forcings in an Oligocene/Miocene Submarine Channel System: Insights From New Age Constraints and Sediment Volumes From the Austrian Northern Alpine Foreland Basin." *Frontiers in Earth Science* 7, no. 302: 1–25.

Hülscher, J., E. R. Sobel, V. Verwater, P. Groß, D. Chew, and A. Bernhardt. 2021. "Detrital Apatite Geochemistry and Thermochronology From the Oligocene/Miocene Alpine Foreland Record the Early Exhumation of the Tauern Window." *Basin Research* 33, no. 6: 3021–3044.

Jiménez-Moreno, G., S. Fauquette, and J. P. Suc. 2008. "Vegetation, Climate and Palaeoaltitude Reconstructions of the Eastern Alps During the Miocene Based on Pollen Records From Austria, Central Europe." *Journal of Biogeography* 35, no. 9: 1638–1649.

Jin, J., T. Aigner, H. Luterbacher, G. H. Bachmann, and M. Müller. 1995. "Sequence Stratigraphy and Depositional History in the South-Eastern German Molasse Basin." *Marine and Petroleum Geology* 12, no. 8: 929–940.

Kuhlemann, J. 2007. "Paleogeographic and Paleotopographic Evolution of the Swiss and Eastern Alps Since the Oligocene." *Global and Planetary Change* 58, no. 1–4: 224–236.

Kuhlemann, J., I. Dunkl, A. Brügel, C. Spiegel, and W. Frisch. 2006. "From Source Terrains of the Eastern Alps to the Molasse Basin: Detrital Record of Non-Steady-State Exhumation." *Tectonophysics* 413, no. 3–4: 301–316.

Kuhlemann, J., and O. Kempf. 2002. "Post-Eocene Evolution of the North Alpine Foreland Basin and Its Response to Alpine Tectonics." *Sedimentary Geology* 152, no. 1–2: 45–78.

Lemcke, K. 1988. *Das bayerische Alpenvorland vor der Eiszeit*. Schweizerbart science publishers.

Maiti, G., A. Koptev, P. Baville, T. Gerya, S. Crosetto, and N. Andrić-Tomašević. 2024. "Topography Response to Horizontal Slab Tearing and Oblique Continental Collision: Insights From 3D Thermomechanical Modeling." *Journal of Geophysical Research: Solid Earth* 129, no. 10: e2024JB029385.

Masalimova, L. U., D. R. Lowe, T. Mchargue, and R. Derksen. 2015. "Interplay Between an Axial Channel Belt, Slope Gullies and Overbank Deposition in the Puchkirchen Formation in the Molasse Basin, Austria." *Sedimentology* 62, no. 6: 1717–1748.

Naylor, M., and H. Sinclair. 2008. "Pro-Vs. Retro-Foreland Basins." *Basin Research* 20, no. 3: 285–303.

Ortner, H., S. Aichholzer, M. Zerlauth, R. Pilser, and B. Fügenschuh. 2015. "Geometry, Amount, and Sequence of Thrusting in the Subalpine Molasse of Western Austria and Southern Germany, European Alps." *Tectonics* 34, no. 1: 1–30.

Ortner, H., F. Reiter, and R. Brandner. 2006. "Kinematics of the Inntal Shear Zone–Sub-Tauern Ramp Fault System and the Interpretation of the TRANSALP Seismic Section, Eastern Alps, Austria." *Tectonophysics* 414, no. 1–4: 241–258.

Ortner, H., C. von Hagke, A. Sommaruga, et al. 2023. "The Northern Deformation Front of the European Alps." In *Geodynamics of the Alps 3: Collisional Processes*, edited by C. L. Rosenberg and N. Bellahsen, 241–312. ISTE-Wiley.

Pfiffner, A. 1986. "Evolution of the North Alpine Foreland Basin in the Central Alps." *International Association of Sedimentologists* 8: 219–228.

Piccolo, A., A. Spang, L. H. Eskens, et al. 2025. "The Dynamics and Surface Signal of Slab Break-Off in Continental Settings: Insights From 3D Numerical Modelling." *Authorea Preprints*.

Quinlan, G. M., and C. Beaumont. 1984. "Appalachian Thrusting, Lithospheric Flexure, and the Paleozoic Stratigraphy of the Eastern Interior of North America." *Canadian Journal of Earth Sciences* 21, no. 9: 973–996.

Ratschbacher, L., W. Frisch, H. G. Linzer, and O. Merle. 1991. "Lateral Extrusion in the Eastern Alps, Part 2: Structural Analysis." *Tectonics* 10, no. 2: 257–271.

Ratschbacher, L., O. Merle, P. Davy, and P. Cobbold. 1991. "Lateral Extrusion in the Eastern Alps, Part 1: Boundary Conditions and Experiments Scaled for Gravity." *Tectonics* 10, no. 2: 245–256.

Rosenberg, C. L., and A. Berger. 2009. "On the Causes and Modes of Exhumation and Lateral Growth of the Alps." *Tectonics* 28, no. 6: 1–16.

Rosenberg, C. L., S. Schneider, A. Scharf, et al. 2018. "Relating Collisional Kinematics to Exhumation Processes in the Eastern Alps." *Earth-Science Reviews* 176: 311–344.

Roure, F. 2008. "Foreland and Hinterland Basins: What Controls Their Evolution?" *Swiss Journal of Geosciences* 101, no. 1: 5–29.

Royden, L. H. 1993. "The Tectonic Expression Slab Pull at Continental Convergent Boundaries." *Tectonics* 12, no. 2: 303–325.

Sabbatino, M., S. Tavani, S. Vitale, et al. 2021. "Forebulge Migration in the Foreland Basin System of the Central-Southern Apennine Fold-Thrust Belt (Italy): New High-Resolution Sr-Isotope Dating Constraints." *Basin Research* 33, no. 5: 2817–2836.

Scharf, A., M. Handy, S. Favaro, S. M. Schmid, and A. Bertrand. 2013. "Modes of Orogen-Parallel Stretching and Extensional Exhumation in Response to Microplate Indentation and Roll-Back Subduction (Tauern Window, Eastern Alps)." *International Journal of Earth Sciences* 102, no. 6: 1627–1654.

Schellart, W. 2017. "A Geodynamic Model of Subduction Evolution and Slab Detachment to Explain Australian Plate Acceleration and Deceleration During the Latest Cretaceous–Early Cenozoic." *Lithosphere* 9, no. 6: 976–986.

Schmid, S., B. Fügenschuh, E. Kissling, and R. Schuster. 2004a. *TRANSMED Transects IV, V and VI: Three Lithospheric Transects Across the Alps and Their forelands. The TRANSMED Atlas: The Mediterranean Region from Crust to Mantle*. Springer Verlag.

Schmid, S. M., B. Fügenschuh, E. Kissling, and R. Schuster. 2004b. "Tectonic Map and Overall Architecture of the Alpine Orogen." *Eclogae Geologicae Helvetiae* 97, no. 1: 93–117.

Schmid, S. M., O.-A. Pfiffner, N. Froitzheim, G. Schönborn, and E. Kissling. 1996. "Geophysical-Geological Transect and Tectonic Evolution of the Swiss-Italian Alps." *Tectonics* 15, no. 5: 1036–1064.

Schmid, S. M., A. Scharf, M. R. Handy, and C. L. Rosenberg. 2013. "The Tauern Window (Eastern Alps, Austria): A New Tectonic Map, With Cross-Sections and a Tectonometamorphic Synthesis." *Swiss Journal of Geosciences* 106, no. 1: 1–32.

Sinclair, H. 1997. "Flysch to Molasse Transition in Peripheral Foreland Basins: The Role of the Passive Margin Versus Slab Breakoff." *Geology* 25, no. 12: 1123–1126.

Sinclair, H., B. Coakley, P. Allen, and A. Watts. 1991. "Simulation of Foreland Basin Stratigraphy Using a Diffusion Model of Mountain Belt Uplift and Erosion: An Example From the Central Alps, Switzerland." *Tectonics* 10, no. 3: 599–620.

Thatcher, W., and F. F. Pollitz. 2008. "Temporal evolution of continental lithospheric strength in actively deforming regions." *Gsa Today* 18, no. 4-5: 4–11.

Trümpy, R. 1960. "Paleotectonic Evolution of the Central and Western Alps." *Geological Society of America Bulletin* 71, no. 6: 843–907.

Turcotte, D. L., and G. Schubert. 2002. *Geodynamics*. Cambridge university press.

Ver Straeten, C. A., and C. E. Brett. 2000. "Bulge Migration and Pinnacle Reef Development, Devonian Appalachian Foreland Basin." *Journal of Geology* 108, no. 3: 339–352.

Verwater, V. F., E. Le Breton, M. R. Handy, V. Picotti, A. Jozi Najafabadi, and C. Haberland. 2021. "Neogene Kinematics of the Giudicarie Belt and Eastern Southern Alpine Orogenic Front (Northern Italy)." *Solid Earth* 12, no. 6: 1309–1334.

Wagner, L. R. 1998. "Tectono-Stratigraphy and Hydrocarbons in the Molasse Foredeep of Salzburg, Upper and Lower Austria." *Geological Society, London, Special Publications* 134, no. 1: 339–369.

Wangen, M. 2010. *Physical Principles of Sedimentary Basin Analysis*. Cambridge University Press.

Waschbusch, P. J., and L. H. Royden. 1992. "Spatial and Temporal Evolution of Foredeep Basins: Lateral Strength Variations and Inelastic Yielding in Continental Lithosphere." *Basin Research* 4, no. 3–4: 179–196.

Zweigel, J., T. Aigner, and H. Luterbacher. 1998. "Eustatic Versus Tectonic Controls on Alpine Foreland Basin Fill: Sequence Stratigraphy and Subsidence Analysis in the SE German Molasse." *Geological Society, London, Special Publications* 134, no. 1: 299–323.

## Appendix A

### A.1 | Time to Depth Conversion

Before converting the seismic from the time to the depth domain, we interpreted the seismics to generate a geological model in the time domain. Where interpreted reflectors in the time domain intersect with boreholes, the true depth is known as well. This allows us to calculate an average velocity from the surface to the respective stratigraphic surface. Doing this for multiple of the interpreted reflectors allows us to calculate average velocities (Table A1). Based on this calculation we find an average velocity of 2678 m/s from the surface up until the top Turonian. This velocity was subsequently used to convert the seismic from the time to depth domain.

### A.2 | Deflection Under a Distributed Load–Numerical Solution of Wangen (2010)

**General equation of flexure:** Many previous studies have treated the continental lithosphere as a linear elastic solid to model the deflection of a subducting plate under mountain topographic load (Sinclair et al. 1991; Gutscher 1995; Andeweg and Cloetingh 1998; Wangen 2010; Allen and Allen 2013). The equation representing the deflection of a linear elastic plate due to vertical loading, in the absence of any horizontally applied forces, has the following form (Allen and Allen 2013).

$$D\frac{d^4w}{dx^4} + \Delta\rho g w = 0 \tag{A1}$$

where $w$ is the deflection, $x$ is the horizontal length, $D$ is the flexural rigidity of the plate, $\Delta\rho$ is the difference in density between mantle $\rho_m$ and infilling material (i.e., sediment) and $\rho_i$.

The flexural rigidity $D$ depends on the elastic thickness ($h$), Young's modulus ($E$), and Poisson's ratio ($\nu$) of the elastic plate and has the relation, $D = \frac{Eh^3}{12(1-\nu^2)}$.

Equation (A1) is commonly used to calculate the flexure of a 2D elastic plate under a vertical load $q(x)$ (Turcotte and Schubert 2002; Allen and Allen 2013). In this approach, the total topographic load $q(x)$ along a 2D mountain profile is assumed to act at a single point on the elastic plate, causing the downward deflection. However, in reality, the mountain topographic load $q(x)$ varies with horizontal distance $x$, and treating it as a point load can be an oversimplification that fails to capture the distributed nature of the mountain load. To address this, the total topographic load can be discretised into a series of individual point loads, and the total deflection of the plate can be approximated using the principle of superposition by summing the responses to these discrete loads.

**TABLE A1** | Average velocities from the surface to interpreted seismic horizon.

| Stratigraphic surface | Average velocity (m/s) | Number of wells |
|---|---|---|
| Base Hall Unconformity | 2709 | 93 |
| Top Chattian Sands | 2516 | 91 |
| Base Eocene | 2729 | 63 |
| Top Turonian | 2739 | 10 |

In our study, we use the semi-numerical solution for the deflection of an elastic plate under a distributed load, provided by Equations 9.49 and 9.50 in Wangen (2010), to model the flexural response of the downgoing European plate due to loading by the Alpine thrust sheets.

**Semi-numerical solution of flexure under series of point loads (Equations 9.49 and 9.50 in Wangen 2010; and Equations A33.1–A33.3 in Allen and Allen 2013):** The distributed load $q(x)$ is treated as a series of blocks of height $h_i$, extending laterally from point $x_i$ to $x_{i+1}$, with a load magnitude $V_i$. The centre of each mountain block is at $x_{i+1} - x_i$. The load of each individual block (weight) in the interval $i$ from $x_i$ to $x_{i+1}$ becomes the point load and it is given by:

$$V_i = \int_{x_i}^{x_{i+1}} q(x)dx = \frac{1}{2}\{q(x_i) + q(x_{i+1})\}(x_{i+1} - x_i) \tag{A2}$$

The deflection $w(x)$ of the downgoing plate is then calculated as the sum of all of the individual deflections under $i = N$ load blocks.

The deflection at any position $x$ is then the sum of all the individual deflections;

$$w(x) = \sum_{i=1}^{N} \frac{V_i}{2\Delta\rho g\alpha} f(u) \tag{A3}$$

where the function $f(u) = \exp(-u)(\cos u + \sin u)$. Here, $u$ is given by.

$$u = |x - x_{c,i}| / \alpha \tag{A4}$$

where $x_{c,i}$ is the position of the centre of each load block, and $\alpha$ is the flexural parameter, $\alpha = \left\{\frac{4D}{\Delta\rho g}\right\}^{1/4}$.

The grouping before $f(u)$ in the summation before is the maximum deflection for each load $V_i$.

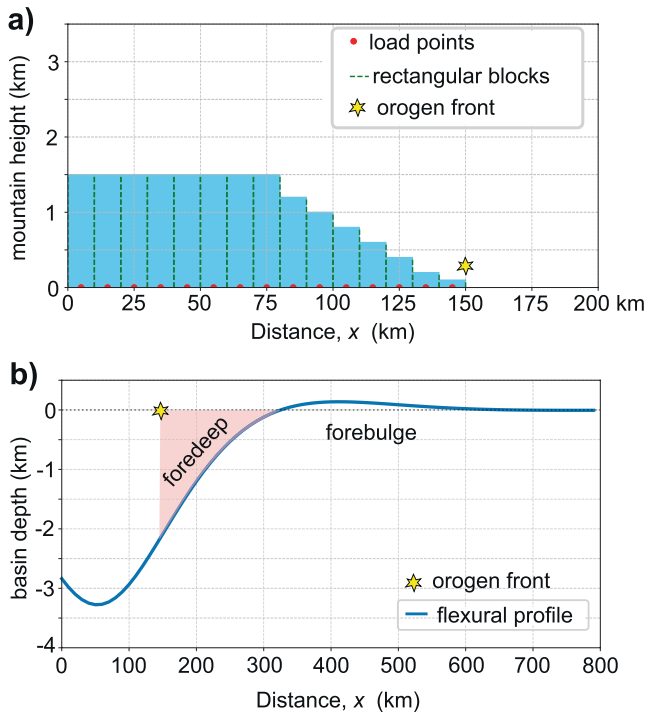


**FIGURE A1** | (a) The distributed load in model M1500 is treated as a series of rectangular blocks of different heights that approximate the mountain topography. At the centre of these rectangular bars, the load acts as a point load. This is how the total topographic load is discretised into a series of individual point loads. (b) The total deflection of the plate is obtained by summing the responses to these discrete point loads. [Colour figure can be viewed at wileyonlinelibrary.com]

For detailed derivation, readers are referred to Equations 9.49 and 9.50 in Wangen (2010) and Equations A33.1–A33.3 in Allen and Allen (2013).